Detection of Water Cloud Microphysical Properties Using Multi-scattering Polarization Lidar

1 author:

Lingbing Bu
Nanjing University of Information Science & Technology
76 PUBLICATIONS   181 CITATIONS

SEE PROFILE

Some of the authors of this publication are also working on these related projects:

Theoretical and experimental research on polarized detection of cloud particle View project

Development of a Mid-infrared DIAL system for pollution gas detection View project

Detection of Water Cloud Microphysical Properties Using Multi-scattering Polarization Lidar

Jiaming Xie[1], Xingyou Huang[1]*, Lingbing Bu[1]**, Hengheng Zhang[1], Farhan Mustafa[1], and Chenxi Chu[2]

[1]*Collaborative Innovation Center on Forecast and Evaluation of Meteorological Disasters,*
Key Laboratory for Aerosol-Cloud-Precipitation of China Meteorological Administration,
Key Laboratory of Meteorological Disasters, Ministry of Education,
Nanjing University of Information Science and Technology, Nanjing 210044, China
[2]*Jiangsu Meteorological Observation Center, Nanjing 210044, China*

Multiscattering occurs when a laser transmits into dense atmosphere targets (e.g. fogs, smoke or clouds), which can cause depolarization effects even though the scattering particles are spherical. In addition, multiscattering effects have additional information about microphysical properties of scatterers. Thus, multiscattering can be utilized to study the microphysical properties of the liquid water cloud. In this paper, a Monte Carlo method was used to simulate multi-scattering transmission properties of Lidar signals in the cloud. The results showed the slope of the degree of linear polarization (SLDLP) can be used to invert the extinction coefficient, and then the cloud effective size (CES) and the liquid water content (LWC) may be easily obtained by using the extinction coefficient and saturation of the degree of linear polarization (SADLP). Based on calculation results, a microphysical properties inversion method for a liquid cloud was presented. An innovative multiscattering polarization Lidar (MSPL) system was constructed to measure the LWC and CES of the liquid cloud, and a new method based on the polarization splitting ratio of the Polarization Beam Splitter (PBS) was developed to calibrate the polarization channels of MSPL. By analyzing the typical observation data of MSPL observation in the northern suburbs of Nanjing, China, the LWC and CES of the liquid water cloud were obtained. Comparisons between the results from the MSPL, MODIS and the Microwave radar data showed that, the microphysical properties of liquid cloud could be retrieved by combining our MSPL and the inversion method.

Keywords : Multiscattering polarization Lidar, Microphysical properties of liquid water cloud, Polarization calibration
OCIS codes : (010.1615) Clouds; (010.3640) Lidar; (290.4210) Multiple scattering

I. INTRODUCTION

Clouds are an important part of the Earth's climate system, and their radiation effect significantly affects the balance of the Earth's radiation budget [1, 2]. Cloud observation is crucial for weather forecasting and aeronautical weather forecasting. Exploring the macro-micro characteristics of clouds is one of the fundamental parts of the study of atmospheric dynamics and thermal processes [3]. The cloud effective size (CES) and liquid water content (LWC) are two important parameters used in the study of microphysical properties of liquid clouds. Due to the limitations of airborne measurement instruments, such as high cost and scarcity of observation opportunities, methods for remote sensing of LWC and CES have become research hotspots in recent years. The active detection of microphysical parameters of cloud can be summarized into three types: the first method is using millimeter wave radar, and then

Color versions of one or more of the figures in this paper are available online.

the empirical formulas are used to invert microphysical parameters of clouds [4]. The second method is using a water vapor Raman Lidar to obtain microphysical parameters of cloud [5]. However, microwave radar has a long wavelength and it is difficult to detect a thin cloud with a small optical thickness, and Raman scattering signal intensity is much smaller than the Mie scattering signal, which makes it impossible to observe during the day. Multiscattering polarization Lidar (MSPL) can overcome the above two shortcomings, and has a good application prospect in observation of cloud microphysical properties [6].

In recent years, important progress has been made in the study of multiscattering effects on Lidar signals. Plat *et al.* used the Monte Carlo method to calculate multiscattering effects and emphasized the importance of multiscattering for cirrus research [7]. Eloranta *et al.* further studied the Lidar echo model affected by multiscattering effects using the approximate radiation transfer theory, Monte Carlo calculation and a random model of the multiscattering process [8]. Cecilia *et al.* studied the importance of multi-scattering effects on Lidar data and demonstrated the correlation between the Monte Carlo method and the depolarized Lidar technique [9]. Bissonette *et al.* simulated the effects of multiscattering using a paraxial approximation radiation transfer process, and compared the radiation transfer process with the measured data in the laboratory [10]. Meglinski *et al.* used the Monte Carlo method to simulate the time-dependent function of coherent backscattered light in a random nonhomogeneous turbid medium, and proved that the optical path of the photon cluster of the nth scattering event directly corresponds to the contribution of the n-hierarchy graph [11]. Tikhomirov *et al.* obtained a correspondence of multiple scattering contribution estimations from experimental data with model ones, and presented calculations of clouds' optical parameters and clouds' effective droplets size from experimental data [12]. Kim *et al.* obtained the effects of different CES and LWC values on the multiscattering of Lidar signals by Monte Carlo simulation. The corresponding relationship between the optical thickness and the degree of polarization of cloud droplets with improved gamma distribution was found. A method for retrieving the microphysical properties of water clouds using SLDLP and SADLP has been proposed [13, 14]. Wang *et al.* used the small angle approximation method to find that multi-scattering is mainly related to the FOV and optical thickness [15]. Sato *et al.* performed a practical modeling of Monte Carlo simulations of multiscattering effects in the clouds to analyze depolarized Lidar echoes generated by inhomogeneous clouds [16]. Zhang *et al.* retrieved the liquid water content (LWC) of clouds using a single-channel multiscattering Lidar system without depolarization information [17]. Okamoto *et al.* used multiple scattering polarization Lidar to observe the depolarization ratios of optically thick low level clouds [18]. At present, most of the studies related to multiscattering focus on theoretical research and there are only a few experimental

studies that deal with real multiscattering signals. Therefore, the experimental study of multiscattering is significant for measurement of the microphysical properties of clouds.

In this paper, we proposed a method to measure LWC and CES by MSPL. Firstly, the Monte Carlo method was used to simulate the Lidar signal under different conditions. It was suggested that SLDLP and SADLP at different FOVs can be used to calculate the liquid water content and the effective particle size of a liquid water cloud. Based on the theoretical studies, a multi-scattering polarization Lidar was built to detect the liquid water cloud, and a new calibration method as well as a cloud inversion method were developed. By analyzing the typical observation samples of MSPL observed in the northern suburbs of Nanjing, China, the LWC and CES of homogeneous liquid water cloud were obtained. Comparisons between the results from the MSPL and other instruments showed that our proposed method is reasonable to invert the microphysical properties of liquid clouds.

II. MONTE CARLO SIMULATION OF MULTIPLE SCATTERING IN CLOUDS

The Monte Carlo method is very helpful in simulating the scattering characteristics of a laser under conditions that are obtained by tracking the random motion of each photon in the medium. These scattering characteristics can be obtained by statistics. In order to track the photons in the simulation process, it is necessary to sample the scattering angle and the step size of the photon random walk. According to the sampling principle, the step size of the random walk is $s = \ln \xi / \sigma$, Where ξ is a homogeneous random number between 0 and 1, and σ is the extinction coefficient of the cloud. In each simulation, the receiving FOV, CES, laser wavelength, number of photons emitted and cloud height (cloud top height and cloud base height) need to be set in advance. The scattering angle and scattering path depend on the random number given by the system. As simulation error becomes large with a small number of emitted photons, it is essential to use a large number of photons to calculate the multiscattering effects of the Mie scattering process [19].

In our simulation, to simplify the model, it was assumed that the cloud was homogeneous. And the particles in liquid water cloud follow the gamma size distribution [20]

$$dN/dr = N_0 r^a e^{-br}, \tag{1}$$

where N(r) is cloud droplet size distribution, N_0 is calculated constant for the water content value for a given value, and a, b are constants associated with CES.

Although there are many kinds of clouds in nature and in most case clouds don't follow the requirement of homogeneousness, a simple homogeneous cloud model is

often used in this area [6]. Moreover, an ideal model can be used as an effective approximation when the laser does not penetrate the cloud deeply. In fact, laser can only penetrate a small part of the cloud because of the strong attenuation of the cloud.

In the process of simulating the properties of liquid water clouds using the degree of linear polarization P_{dlp}, the slope of the degree of linear polarization (SLDLP) and the saturation of the degree of linear polarization (SADLP) are introduced. The degree of linear polarization P_{dlp} is expressed as

$$P_{dlp} = \frac{I_P - I_R}{I_P + I_R} \approx P_{dp} = \frac{\sqrt{Q^2 + U^2 + V^2}}{I}, \qquad (2)$$

where I_P and I_R represent the linear polarization of the Lidar echo signal in the parallel direction and in the vertical direction, I, Q, U, and V are components of the Stokes vector.

The variation in degree of linear polarization and Ratio of Multiple and Single scattering (RMS) with the depth of cloud at different FOVs is studied. Laser divergence angle, laser wavelength, extinction coefficient, CES size and cloud base height were set to 1 mrad, 532 nm, 5 km^{-1}, 10 m and 1 km respectively. The simulation results were shown in Fig. 1. When the laser reaches the base of the cloud, the degree of linear polarization is 1, indicating that the laser at the initial moment is linearly polarized. As the depth of

cloud increases, the initial linear polarization will decrease rapidly, and then slowly approach a saturation value. This is the depolarization effect in multiscattering processes. The definitions of SLDLP and SADLP mentioned above were also shown in Fig. 1, where SLDLP was defined as the slope of the linear degree of polarization and SADLP is defined as the saturation of the linear degree of polarization. The linear degree of polarization can be calculated using the depolarization ratio measured by Lidar. Then SLDLP and SADLP can be linearly fitted using a least square method. It is obvious that the value of SLDLP is constant and does not change with the FOV, and the larger the FOV, the smaller will be the SADLP value. The RMS is defined as the ratio of the energy of multi-scattering in the total scattering energy. It can be seen from the figure that the RMS is 0 at the base of the cloud. As the penetration depth increases, the RMS will increase rapidly, and then slowly reach a saturation value which is proportional to FOVs. By comparing the value of linear polarization and RMS with the depth of cloud penetration at different fields of view, it can be concluded that the depolarization phenomenon in the backscattering echo signal of liquid water cloud is caused by multiscattering effects.

According to above result, we determined that multi-scattering is the main reason for depolarization of a liquid water cloud. So, we can say that depolarization caused by multi-scattering brings more information about cloud micro-physical characteristics. So we examined the relationship
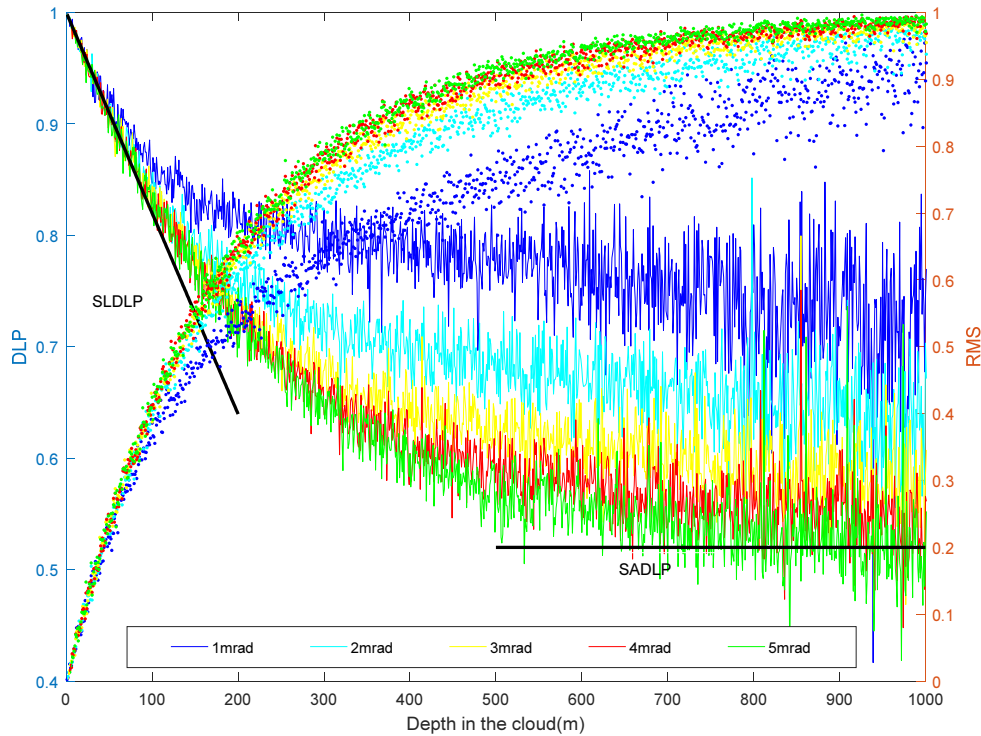

FIG. 1. P_{dlp} (solid line) and RMS (scatter) as a function of height and FOV (extinction coefficient = 5 km^{-1}, CES = 10 um, λ = 532 nm, LBD (Laser Beam Divergence) = 1 mrad, cloud base: 1000 m, cloud top: 2000 m).

between this kind of depolarization and cloud microphysical characteristics.

In the process of Monte Carlo simulation, we get SLDLP and SADLP under different conditions by setting different parameters. It is found that the SLDLP is only related to the extinction coefficient. SADLP not only changes with extinction coefficient, but also changes with CES. The law between SLDLP and extinction coefficient satisfies the following relationship [14]

$$\text{SLDLP} = a\alpha^2 + b\alpha + c, \tag{3}$$

where α denotes the extinction coefficient in terms of km^{-1}, a, b, c are coefficients of the equation and are determined by other parameters.

According to the above results of Monte Carlo simulation, a method for retrieving LWC and CES using MSPL is proposed. Firstly, SLDLP and SADLP at different FOV are obtained from Lidar signals. Then, the extinction coefficient of the cloud is calculated by averaging SLDLP with different FOV. After the extinction coefficient is determined, CES can be inverted by SADLP from different FOV. Finally, LWC is calculated based on the known extinction coefficient and CES.

III. LIDAR SYSTEM

A Monte Carlo method was used to simulate the multiple scattering of a liquid water cloud with small particle size, and the results were shown in Fig. 2. We found that the multiple scattering effect is not significant when the laser enters the liquid water cloud with small optical thickness. The proportion of multiple scattering in the received Lidar signal with small FOV is low, and the information of cloud microphysical characteristics contained in it is not sufficient. The proportion of multiple scattering in the signals received
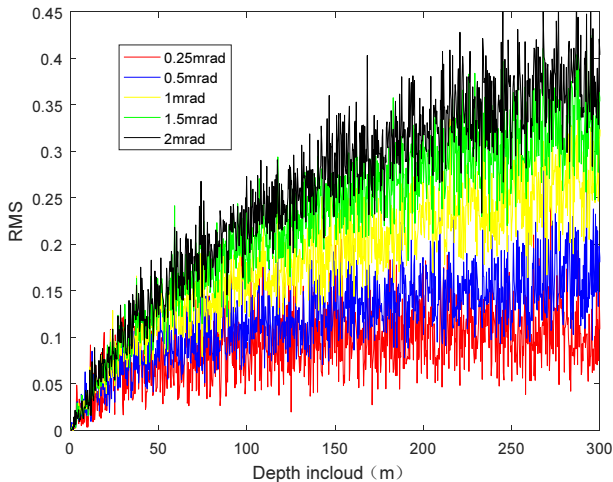
by Lidar with large FOV is higher, and the information of cloud microphysical characteristics can be extracted more accurately. Considering only multiple scattering, the FOV of Lidar should be increased as much as possible. However, with the increase of FOV, the proportion of background noise in the signal received by the telescope becomes higher. In order to realize all day observation of multiple scattering polarization Lidar, it is necessary to limit the
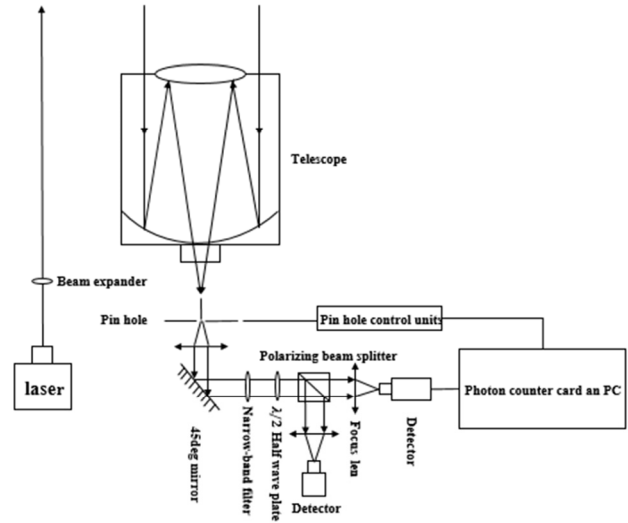

FIG. 3. Schematic diagram of multi-scattering polarization Lidar.

TABLE 1. Key parameters and specifications of MSPL

Typical parameter	Value
Laser emission	
Laser	Semiconductor laser
Wavelength	532 nm
Pulse repetition frequency	1 kHz
Pulse energy	100 uJ
Beam expander	3x adjustable
Receiving and detecting	
Telescope	Cassegrain
Diameter	200 mm
Focal length	2000 mm
Filter	
CWL	532 ± 0.05 nm
Bandwidth	0.3 nm
Peak transmittance	70%
Signal Acquisition	
PMT	H10682-110
Photon counting card	P7882
Sampling frequency	200 MHZ

FIG. 2. RMS at different FOVs.

FOV to suppress the sky background noise signal. To ensure both the multiple scattering ratio and the signal-to-noise ratio of the Lidar signal, we designed a set of multiple scattering polarization Lidar with adjustable FOV.

The schematic diagram of the system is shown in Fig. 3. The MSPL consists of a transmitting system, a receiving system, and a signal processing system. The transmitting system employs a compact Nd:YAG laser as the light source that generates a second harmonic at 532 nm and the repetition rate and pulse energy of the laser are 1 KHz and 100 µJ, respectively. The laser beam divergence is compressed to 0.25 mrad by using an adjustable beam expander. The receiving system uses a Cassegrain telescope with a diameter of 200 mm and a focal length of 2000 mm. The collected scattered light is detected by the photomultiplier tube (PMT) after being collimated, filtered and split by a polarization beam splitter (PBS). Then the backscattered light can be converted into electrical signal by the PMT which can be acquired and recorded by the photon counter card. Table 1 lists the parameters of each component of MSPL.

The main difference between MSPL and the traditional Lidar is that in MSPL, we place a variable aperture electromotive pin hole on the focal plane of the receiving telescope to realize multi-FOVs detection. By adjusting the aperture size of the pin hole through the host computer software, the Lidar signals with different FOVs can be obtained. The aperture size can be varied from 0.5 mm to 7 mm with a minimum controllable step size of 50 nm. So FOV can vary from 0.25 mrad to 3.5 mrad on the basis of a telescope focal length that is 2000 mm. Currently MSPL mainly used to measure the microphysical properties of liquid water clouds.

Because the receiving efficiency of PMTs are different and the polarization beam splitter (PBS) doesn't match the polarization state of the emitted laser, calibration of the polarization Lidar is necessary. Freudenthaler *et al*. proposed that the calibration process of polarized Lidar can be done by rotating a half-wave plate placed in front of the PBS [21]. Bu *et al*. proposed to scale the polarization constant based on the Jones matrix [22]. However, these methods are difficult to implement, and it is necessary to adjust the optical axis of the half-wave plate parallel to the polarization plane of the PBS. Hence, we proposed a calibration method that can divide the calibration parameters into gain ratio of PMT and the leakage ratio of PBS. By changing places of the two PMTs, the two parameters can be solved separately. The calibration method is described as follows: As shown in Fig. 4, the backscattered signal received by the telescope is collimated and filtered, and then enters the PBS. If the mismatch between the PBS and the half-wave plate is ignored, the optical signals received by the two channels after passing through the PBS are $P_\parallel$ and $P_\perp$ respectively, and depolarization ratio is expressed as $\delta = P_\perp / P_\parallel$. Due to the mismatch between the PBS and
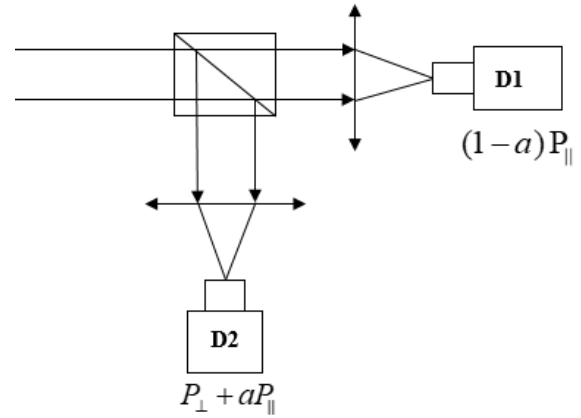

FIG. 4. Schematic diagram of a polarized Lidar.

half-wave plate, the parallel channel light will leak into the vertical channel, and vertical channel light will leak into the parallel channel. However, since the optical signal of the vertical channel is weak, the light leaking into the parallel channel is negligible. Considering the leakage of the two channels, the optical signals received by the two channels are $(1-a)P_\parallel$ and $P_\perp + aP_\parallel$. The receiving efficiency ratio of two PMTs satisfies G = KD1/KD2 (KD1 is the receiving efficiency of the PMT in the parallel channel, and KD2 is the receiving efficiency of the PMT in the vertical channel), so the following two equations are satisfied before and after the exchange of the two PMTs. Where δ_{raw1} and δ_{raw2} are the original depolarization ratios before and after the exchange.

$$\delta_{raw1} = \frac{P_\perp + aP_\parallel}{(1-a)P_\parallel} \frac{1}{G}, \tag{4}$$

$$\delta_{raw2} = \frac{P_\perp + aP_\parallel}{(1-a)P_\parallel} G. \tag{5}$$

Eq. (5) is divided by Eq. (4):

$$G^2 = \frac{\delta_{raw2}}{\delta_{raw1}}. \tag{6}$$

Divide the numerator and denominator in Eq. (5) by $P_\parallel$. and deform this equation to get

$$a = \frac{G\delta_{raw} - \delta_0}{1 + G\delta_{raw}}, \tag{7}$$

where δ_{raw} is the raw depolarization ratio and is the same as δ_{raw2}. δ is the corrected depolarization ratio. In this case, it means the depolarization ratio of atmospheric molecules and its value is 0.0036 [23].

We can calculate the value of a by Eq. (7), and then deform this equation to

$$\delta = (1-a) \cdot G\delta_{raw} - a, \qquad (8)$$

where a and G are system constants and do not change with the weather. Therefore, after the calibration constant is determined by experiments, we can use Eq. (8) to correct the depolarization ratio.

Based on this calibration method, we performed the calibration experiment in clear atmospheric conditions after rain. Since this method needs the depolarization ratio of the atmospheric molecules to be used as a calibration basis, so it is required there should be less aerosol at calibrate height. The extinction coefficient of aerosol can be used to determine whether the calibration area is clean. The results are shown in Fig. 5(a), where the red curve represents the backscattering coefficient of the molecule (BCM) and the blue curve represents the backscattering coefficient of the aerosol (BCA). This figure shows that the backscatter coefficient of aerosol is smaller than the backscattering coefficient of atmospheric molecules, so it can be proved that there is almost no aerosol at this height. The gain ratio G = 0.649 was calculated by using
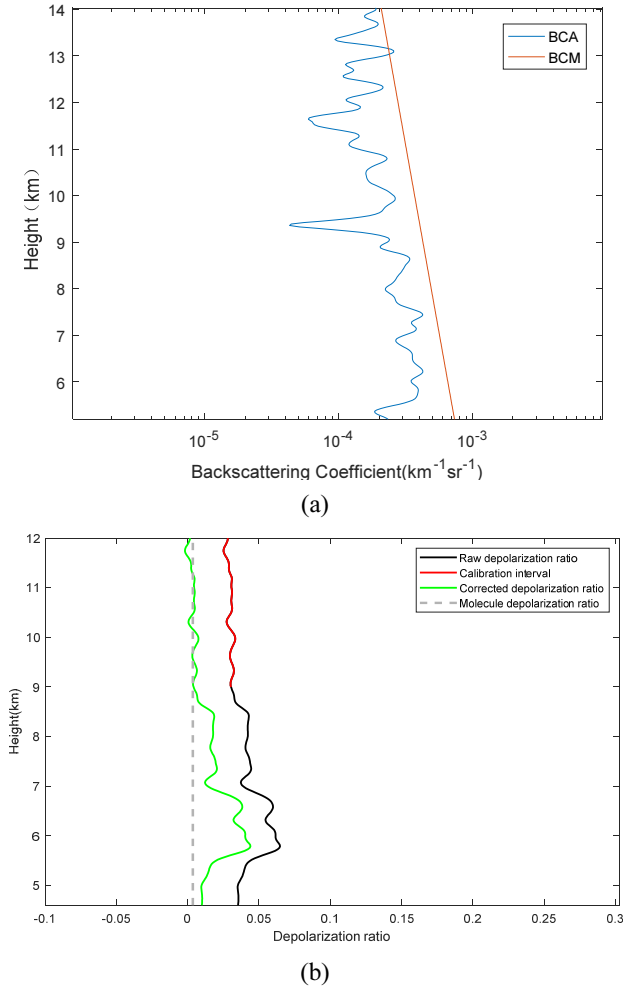

(a)

(b)

FIG. 5. (a) Aerosol backscatter coefficient profile, (b) Calibration results of MSPL.

the measured data. According to the signal ratio of two channels combined with the aerosol backscatter coefficient profile, we selected the height from 5 km to 6.5 km as the calibration area. According to the Eq. (7), a = 0.0253 was calculated, and then the depolarization ratio after the calibration can be calculated by using the Eq. (8). In Fig. 5(b), the blue line indicates the uncalibrated depolarization ratio, the red curve indicates the linear depolarization ratio after calibration, and the gray curve indicates the atmospheric molecular depolarization value. It can be seen from the figure that the depolarization ratio after calibration is close to the depolarization ratio of the molecules, indicating that the calibration experiment is effective. Experimental results show that a and G do not change with the field of view. Therefore, the calibration is the same for all fields of view.

IV. INVERSION OF MICROPHYSICAL PARAMETERS OF LIQUID WATER CLOUD USING MSPL

A series of observation experiments were carried out in the northern suburbs of Nanjing, China (118.72°E, 32.20°N) from 2017 to 2019 using MSPL. Typical data was selected to further study the microphysical properties of liquid water clouds. During these observations, LBD, vertical resolution and accumulative time for one FOV were 0.25 mrad, 30 m and 24 s, respectively. The size of the variable pinhole was set to be 1.5 mm, 2 mm, and 2.5 mm corresponding to the FOV of 0.75 mrad, 1.5 mrad, and 1.25 mrad, respectively.

Figure 6(a) shows the range correction signals of the horizontal channels at three FOVs of 0.75 mrad, 1 mrad and 1.25 mrad observed on May 24, 2017, at 20:12. It is shown that these three curves have the same trend, and the height of the cloud is about 6950 meters above ground. Figure 6(b) shows depolarization ratio as a function of height. It can be seen from the comparison with Fig. 6(a) that the depolarization ratio of the cloud is 0.08 which is less than 0.1. According to reference [24], the depolarization range of ice clouds is between 0.3 and 0.5, so we can determine that the detected clouds are liquid water clouds.

Monte Carlo simulation shows that the depolarization effect caused by multiscattering changes with FOV. We selected the observation data from three different FOVs to calculate the degree of polarization which varied with the laser penetration depth.

Figure 7 shows the DLP as a function of penetration depth when the FOVs are 0.75 mrad, 1 mrad and 1.25 mrad. There are some broken cloud flocs or water vapor layers with high concentration in the cloud bottom. When the receiving field angle is small, the telescope can not receive the multiple scattering generated by it. When using large field of view, the telescope can receive multiple scattering signals. The larger the field of view is, the more multiple scattering signals are received. This indicates that the DLP is not at the same cloud bottom.
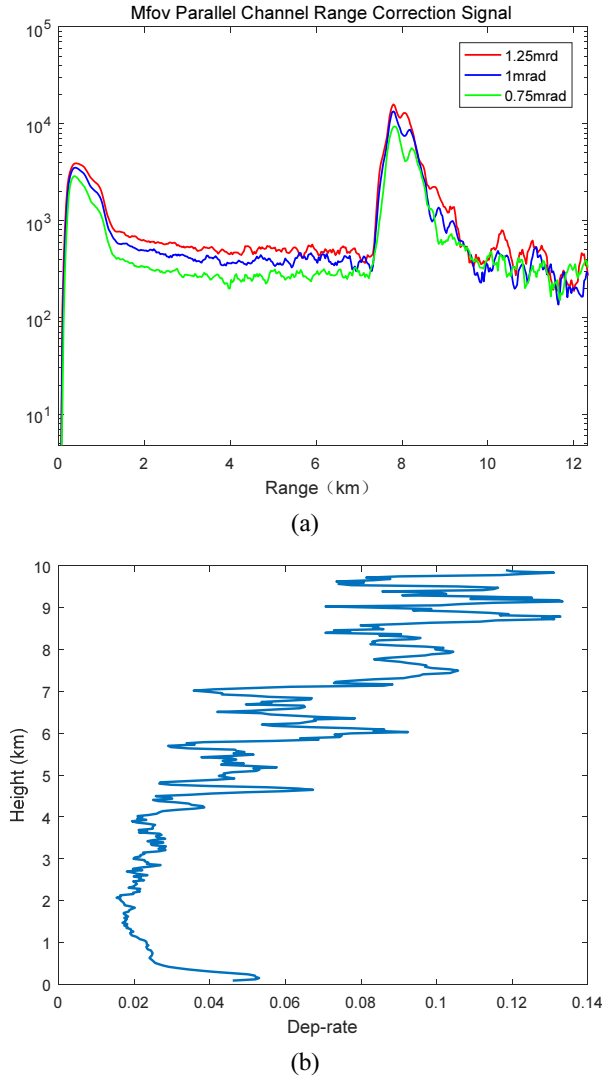
(a)

(b)

FIG. 6. (a) Multi-FOV range correction signal, (b) Depolarization ratio profile at 0.5 mrad.
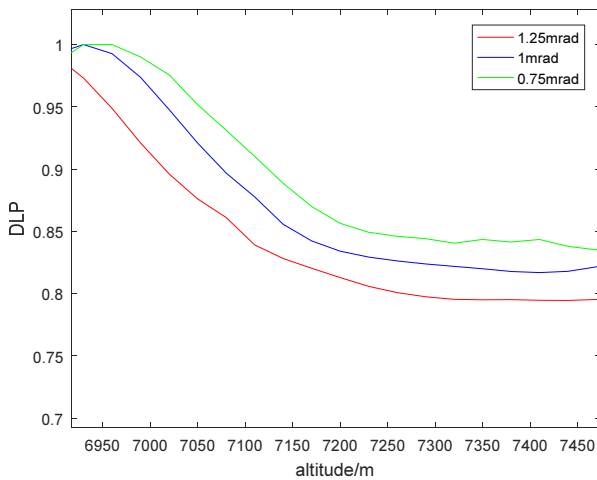

FIG. 7. DLP measured by MSPL.

TABLE 2. Values of SLDLP and SADLP at different FOV

FOV	SLDLP	SADLP
0.75 mrad	-0.7206	0.841
1 mrad	-0.7225	0.817
1.25 mrad	-0.7241	0.795

It can be seen that as FOV increases, the DLP at the same height decreases because the larger the FOV, the greater will be the proportion of multiscattering. Since the DLP variation is linear, we can assume that the CES in the study area is uniform. DLP decreases rapidly with the increase of penetration depth in the cloud. SADLP decreases with FOV, while SLDLP hardly changes with the angle of view. Therefore, we can use SLDLP to retrieve the extinction coefficient.

The fitted SLDLP and SADLP are shown in the Table 2:

In order to avoid the deviation of the SLDLP at single FOV, we calculated the extinction coefficient using the average of the SLDLP at three FOVs. Based on calculation, SLDLP obtained at 0.75 mrad, 1 mrad and 1.25 mrad are -0.7206, -0.7225 and -0.7241 respectively. So, the average value of SLDLP was -0.722.

Flow chart of the inversion method for a liquid cloud is shown in Fig. 8. SLDLP is only related to the extinction coefficient of the cloud, and has no relationship with CES. The law between the above two is as shown in Eq. (3), and the values of a, b, and c are obtained by Monte Carlo simulation [14]. After calculating the values of SLDLP and SADLP, we can invert CES and LWC according to the steps in Fig. 8. In the simulation process, we set the parameters such as CB (cloud base), LBD, laser wavelength and FOV to 6950 m, 0.25 mrad, 532 nm and 1 mrad respectively, and kept them consistent with the real observations. Using different extinction coefficients and corresponding SLDLP, we determined that SLDLP and extinction coefficient fit the following description

$$\text{SLDLP} = 0.002841 * \alpha^2 - 0.2401\alpha - 0.06818, \qquad (9)$$

where α denotes extinction coefficient.

By putting a value of SLDLP = -0.722 into Eq. (9), and calculated cloud extinction coefficient that was 3.166 km^{-1}.

In the process of Monte Carlo simulation, we found that when the extinction coefficient is constant, the relationship between LWC and CES is linear [17]. After the extinction coefficient of the cloud was determined, we simulated the relation between LWC and CES using Monte Carlo simulation with extinction coefficient being 3.166 km^{-1}, as shown in Fig. 9. In terms of mathematics expression, the linear relationship between LWC and CES is satisfied

$$\text{LWC} = 0.00103 * \text{CES} - 0.00036, \qquad (10)$$

where LWC represents the liquid water content in g/m^3, and CES represents the cloud effective size in μm.

The system parameters in the experiment were taken into the Monte Carlo simulation process to calculate the SADLP at different FOVs when the CES took different values. By comparing the SADLP value obtained by the Monte Carlo method with the experimental results, it was determined that the simulated values were closest to the experimental values. When the CES was 22 um, the simulated SADLP is the closest to the measured SADLP, so we determined the CES of this example is 22 um. Then according to Eq. (9), LWC was calculated to be 0.0218 g/m^3. The simulated SADLP and measured values at different FOVs were compared and the results of the inversion were verified.
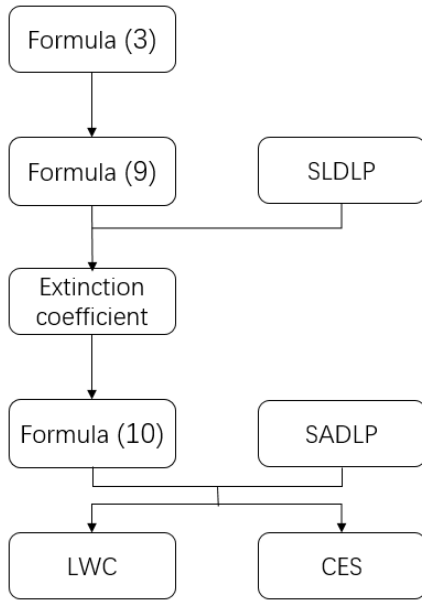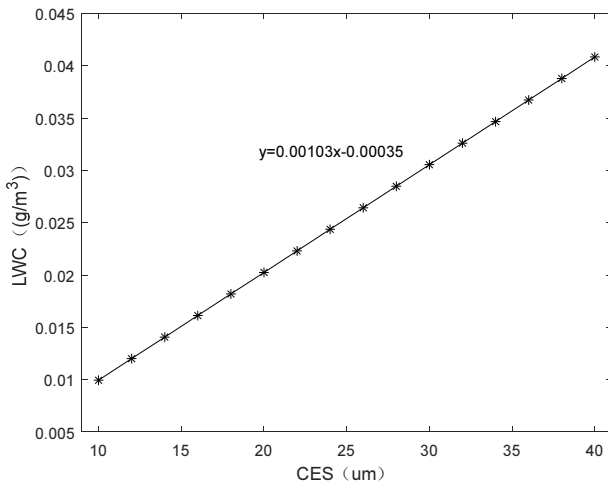

FIG. 8. Flow chart of inversion method.

FIG. 9. Relationship between LWC and CES ($\alpha = 3.166$ km^{-1}).

Figure 10 shows the DLP of the observed data and the DLP of the simulated data as a function of penetration depth in different FOV. In order to facilitate the comparison of the measured and simulated values, we modify the height of DLP = 1 at different FOVs in the same position. The CES set in the Monte Carlo simulation is 21.5 μm and the LWC is 0.0218 g/m^3. The other parameter settings are as same as those real observations. The green, red and blue lines represent the DLP obtained by Monte Carlo simulation at 0.75 mrad, 1 mrad and 1.25 mrad, respectively, and the scatter indicates the DLP obtained from the actual observation data.

We also invert the low level liquid water cloud. On October 14, 2019, we observed water clouds with cloud bottom height varying between 600 m and 800 m, and selected two sets of data for analysis. The following figure shows two group of multi-FOV signals selected at different times. We chose the observation data satisfying our theoretical model as far as possible to further study the microphysical characteristics of liquid water clouds. We extract the liquid water cloud signal and calculate the LWC and the CESs according to the above method. Figures 11 and 12 show the original signal and DLP of the two group data respectively.

According to the Monte Carlo simulation results, under the condition of cloud height, the relationship between SLDLP and cloud extinction coefficient α is described by the following equation:

$$SLDLP = 0.008419*\alpha^2 - 0.5\alpha + 0.6954. \quad (11)$$

Table 3 shows the calculated SLDLP and SADLP at different FOVs of two group data. The calculated mean SLDLP is -2.422 and -2.934 respectively. According to the calculation, we get the average extinction coefficients of 7.08 km^{-1} and 8.47 km^{-1}. On this basis, we calculate the CES and LWC of liquid cloud using the same method.

We get that when the cloud particle radius is 60 μm and 52 μm respectively, the simulation data is closest to

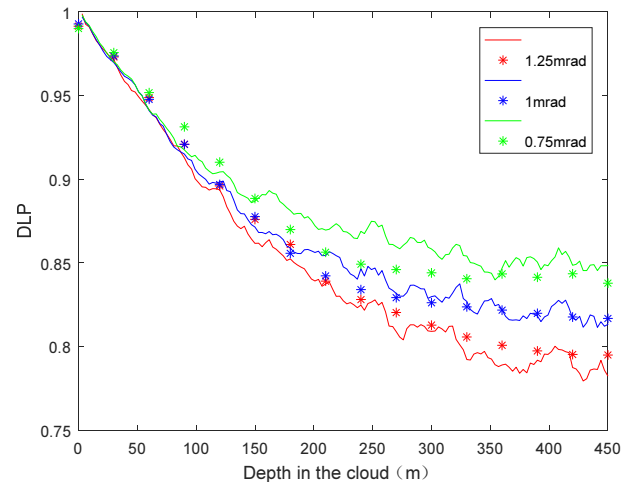FIG. 10. Comparison of measured DLP and simulated DLP.

(a)   (b)

FIG. 11. Original signal and DLP of group1.

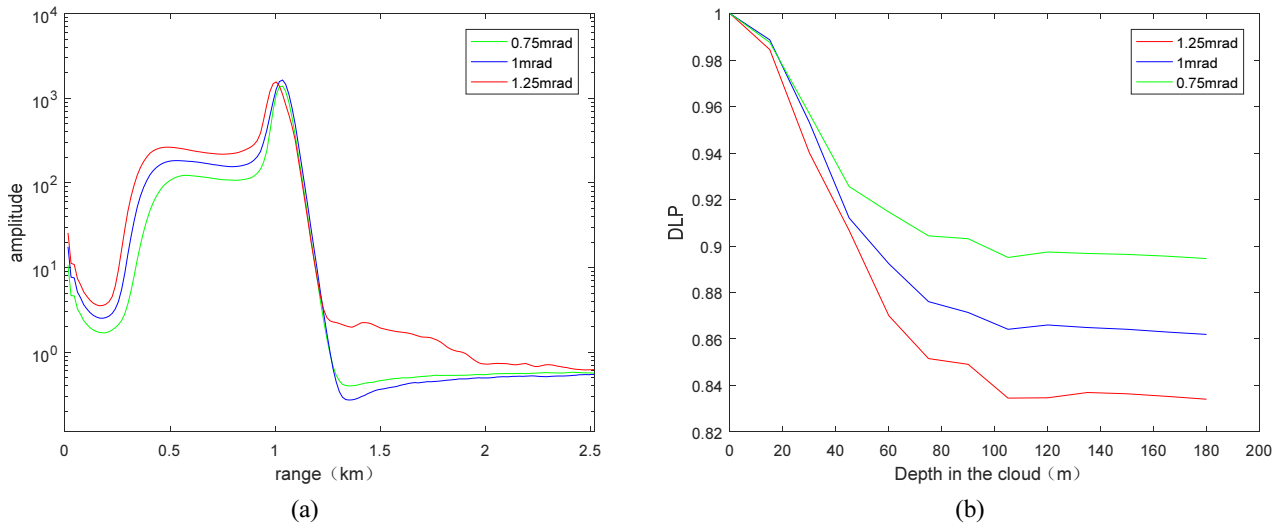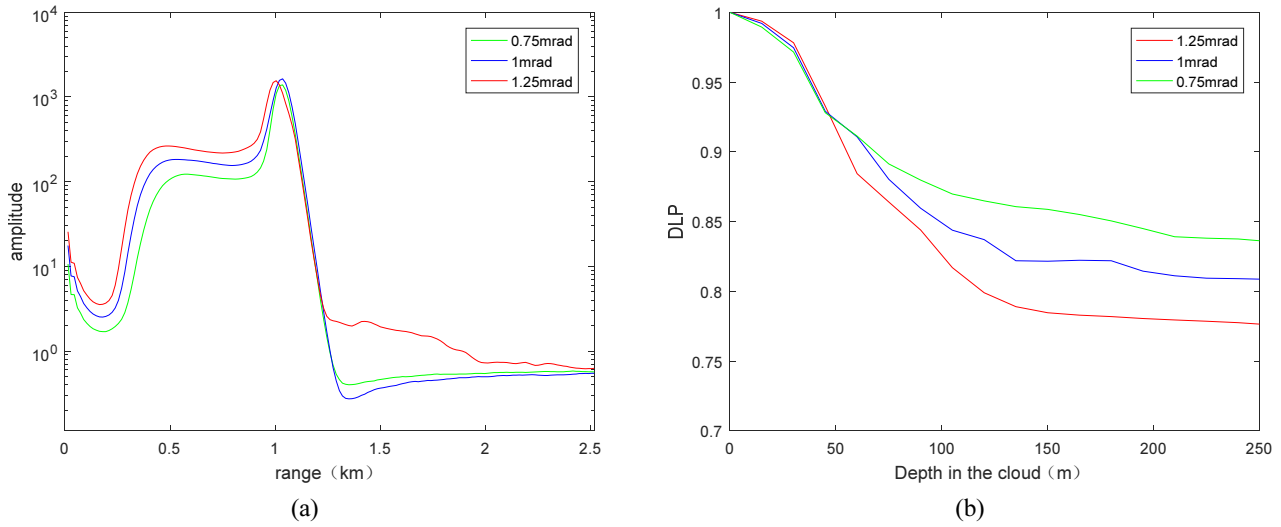(a)   (b)

FIG. 12. Original signal and DLP of group2.

TABLE 3. Values of SLDLP and SADLP at different FOV of two group data

FOV	SLDLP (group1)	SADLP (group1)	SLDLP (group2)	SADLP (group2)
0.75 mrad	-2.133	0.892	-3.001	0.845
1 mrad	-2.527	0.869	-2.867	0.82
1.25 mrad	-2.607	0.834	-2.935	0.781

the observation data, so the cloud particle radius of these two examples is 60 μm and 52 μm respectively. The corresponding liquid water content is 0.15 g/m^3 and 0.163 g/m^3 respectively. Figures 13(a) and 13(b) show the measured DLP and the simulated DLP at different FOV of two group data.

Although the simulation data was very close to the real observation data, there are some possible errors, which were mainly caused by the following reasons: (1) The observation data of the three FOVs were not measured at the same time, and were considered to be measured at the same time in actual processing. (2) Unstable instrument performance, uneven cloud structure, etc. might affect the data quality. (3) The Monte Carlo simulation was based on the ideal conditions under some assumptions, while the meteorological conditions encountered in the real observation were more complicated.
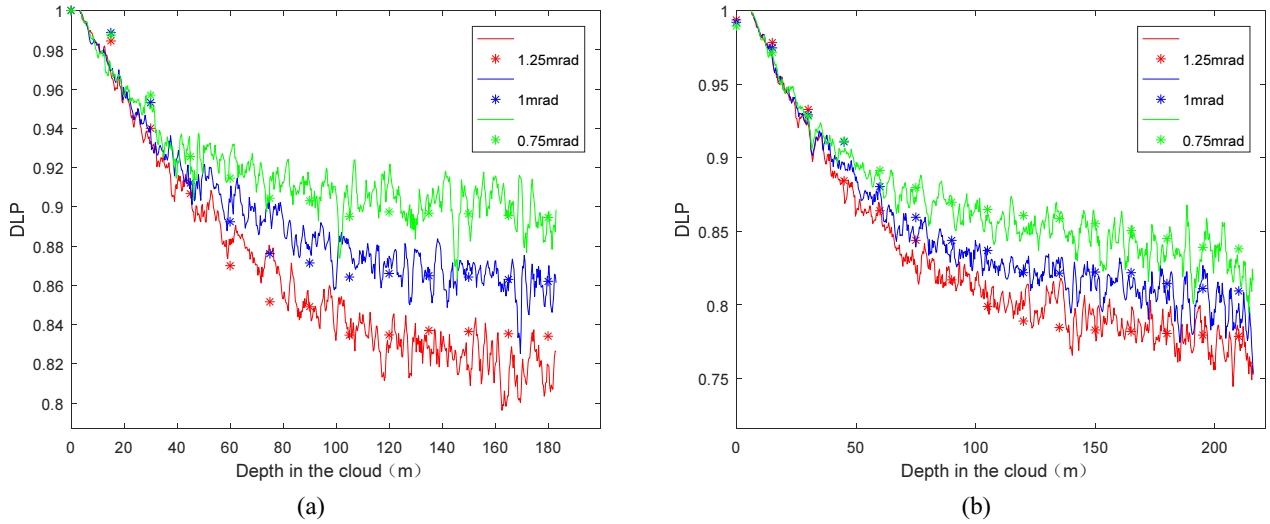
(a)   (b)

FIG. 13. Comparison of measured DLP and simulated DLP of two group data.

V. CONTRAST AND VALIDATE

In order to verify the accuracy of this method, we compared CES and LWC measured by MSPL with the data products of Nanjing Microwave Radar and MODIS. MODIS is a large-scale space remote sensing instrument developed by NASA to understand the global climate change and the impact of human activities on the climate. The device captures data in 36 mutually matched spectral bands, covering from visible to infrared. Provide observation data of the earth's surface once every 1-2 days. They are designed to provide a wide range of global data dynamic measurements, including changes in cloud cover, changes in Earth's energy radiation, ocean land and low-level changes. MODIS can directly provide the average effective radius of liquid water cloud of level 3 data products.

The Microwave Radar is located in Longwangshan, Nanjing, Jiangsu Province, and is about 2 km away from the Lidar observation position. Radar reflectivity Z (mm^6 m^{-3}) is related to liquid water content M (in cm^3 m^{-3}) according to so called Z-M relationship.

$$Z = cM^d, \qquad (12)$$

where constants: c = 24000; d = 1.82. [25]

Figure 14 shows the LWC and radar reflectivity obtained by the Nanjing radar at the same time, and at that time the radar elevation angle was 19.5°. The location of MSPL is marked with a triangle, and the red circle is the position where the cloud is located. From the Fig. 15, the LWC is about 0.02 g/m^3, which is roughly the same as the LWC obtained by the MSPL.

Figure 15 is the daily average data of effective particle radius of a liquid water cloud obtained by MODIS, and the selected research area (Region 118E, 32N, 119E, 33N) is the latitude and longitude corresponding to the Lidar

station. It can be seen from the figure that the average CES of the liquid water cloud on May 24, 2017 is 28 um, so we can also consider that the Lidar data is consistent with MODIS data.

The inconsistency between Lidar and MODIS and microwave radar in the inversion results may be caused by the following reasons: (I) the time deviation of observation, (II) the observation cases are not uniform enough in the horizontal direction, (III) the scattering cross section difference caused by the wavelength inconsistency. It is difficult to measure the microphysical characteristics of a cloud accurately by remote sensing. And the empirical formulas are used to get the microphysical characteristics of cloud by microwave radar, which need to be further confirmed to improve its usability. In summary, as compared to microwave radar and MODIS, MSPL has certain advantages in studying the microphysical properties of liquid water clouds: (1) MSPL can obtain data with high spatial and temporal resolution. (2) MSPL can perform long-term continuous observation on a specific research area to study its changing properties, which can
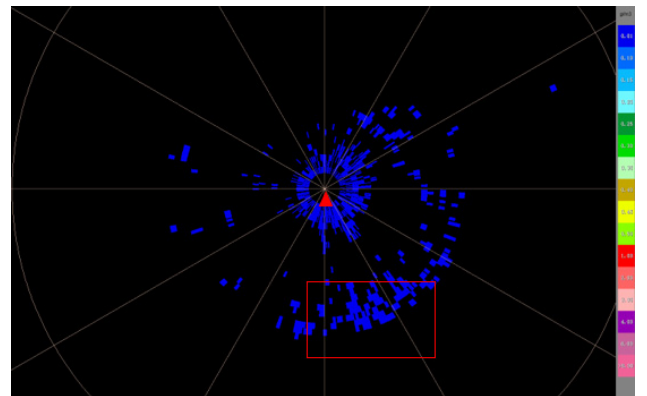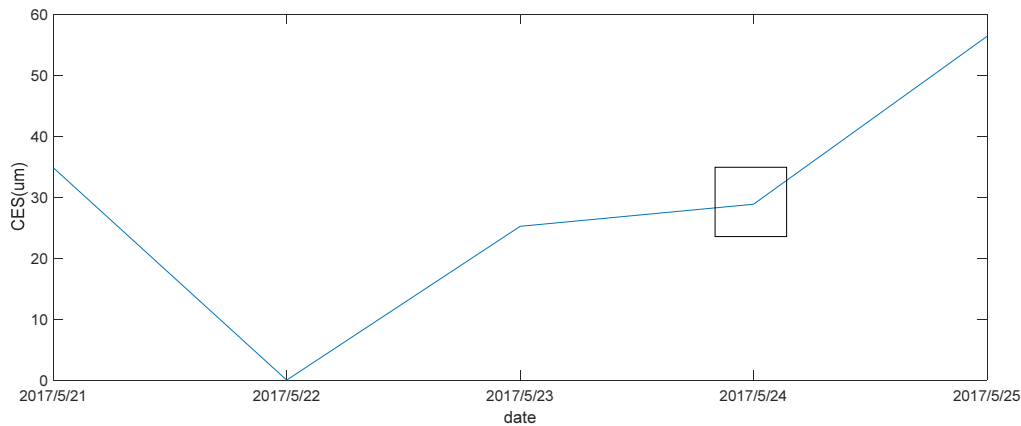

FIG. 14. LWC of microwave radar.

FIG. 15. Area-averaged of liquid water cloud effective particle radius: mean of daily mean daily 1 deg. [MODIS-Terra MOD08_D3 v6.1] microns over 2017-05-21 - 2017-05-25, Shape China, Region 118E, 32N, 119E, 33N.

provide raw data accumulation for small and medium scale numerical weather prediction.

Compared with other remote sensing instruments, the feasibility of using multiple scattering polarization Lidar to retrieve the microphysical characteristics of a liquid water cloud is verified.

VI. CONCLUSION

The variation of DLP with the field of view, extinction coefficient and CES are simulated by using a Monte Carlo method. Based on the simulation results, a method is proposed to invert the microphysical properties of liquid water clouds by using the multiple scattering of clouds. On the basis of theoretical analysis, an MSPL is constructed to detect the liquid water cloud, and a new calibration method is used to calibrate its polarization channels. We use MSPL to observe the liquid water cloud in the northern suburb of Nanjing, and retrieve the microphysical characteristics of a typical example. Firstly, SLDLP and SADLP of different FOV are obtained by fitting the observation data of MSPL. Then, the average SLDLP of different fields of view is used to calculate the extinction coefficient of the cloud. After the extinction coefficient is determined, CES can be extracted from different FOV by SADLP. Finally, LWC is calculated based on the known of extinction coefficient and CES. The results from the MSPL, MODIS and the microwave radar are also compared. The comparison shows a reasonable agreement and consistency to some extent producing some bias, which again verifies the feasibility of method for the retrieving LWC and CES of a liquid water cloud using MSPL. MSPL can be used to measure the microphysical characteristics of water clouds with high temporal and spatial resolution. And MSPL can be also used in measuring the microphysical properties of other particles like fog or cirrus cloud in the future.

REFERENCES

1. A. Sinha, "Effect of atmospheric gases, surface albedo and cloud overlap on the absorbed solar radiation," Ann. Geophys. **14**, 329-335 (1996).
2. M. Degünther and R. Meerkötter, "Effect of remote clouds on surface UV irradiance," Ann. Geophys. **18**, 679-686 (2000).
3. G. L. Stephens, "Cloud feedbacks in the climate system: a critical review," J. Clim. **18**, 237-273 (2005).
4. C. L. Liu and A. J. Illingworth, "Toward more accurate retrievals of ice water content from radar measurements of clouds," J. Appl. Meteorol. **39**, 1130-1146 (2000).
5. D. N. Whiteman and S. H. Melfi, "Cloud liquid water, mean droplet radius, and number density measurements using a Raman Lidar," J. Geophys. Res. **104**, 31411-31419 (1999).
6. S. Xianming, X. Sai, W. Long, W. Haihua, and S. Jin, "Monte Carlo simulation of polarization Lidar multiple scattering by multi-layer discrete random media," Chin. J. Laser **42**, 270-276 (2015).
7. C. M. R. Platt, "Remote sounding of high clouds. III: Monte Carlo calculations of multiple-scattered lidar returns," J. Atmos. Sci. **38**, 156-167 (1981).
8. E. W. Eloranta, "Practical model for the calculation of multiply scattered Lidar returns," Appl. Opt. **37**, 2464-2472 (1998).
9. M. Cecilia, M. C. D. Galvez, R. C. Macatangay, I. B. T. Lim, and E. A. Vallar, "Analysis of the multiple scattering effects on clouds using Monte Carlo and depolarization Lidar method," in *Proc. Technical Digest. CLEO/Pacific Rim '99. Pacific Rim Conference on Lasers and Electro-Optics (Cat. No.99TH8464)* (Seoul, Korea, Aug. 1999).
10. L. R. Bissonnette, G. Roy, L. Poutier, S. G. Cober, and G. A. Isaac, "Multiple-scattering Lidar retrieval method: tests on Monte Carlo simulations and comparisons with *in situ* measurements," Appl. Opt. **41**, 6307-6324 (2002).

11. I. V. Meglinski, V. L. Kuzmin, D. Y. Churmakov, and D. A. Greenhalgh, "Monte Carlo simulation of coherent effects in multiple scattering," Proc. R. Soc. A **461**, 43-53 (2005).

12. A. I. Abramochkin and I. I. Razenkov, "Analysis of a multiple scattering Lidar return from droplet clouds," Proc. SPIE **6160**, 61601F (2006).

13. D. Kim, H. D. Cheong, Y. Kim, S. Volkov, and J. Lee, "Optical depth and multiple scattering depolarization in liquid clouds," Opt. Rev. **17**, 507-512 (2010).

14. D. Kim and J. Lee, "Measuring cloud droplet effective radius and liquid water content using changes in degree of linear polarization along cloud depth," Opt. Lett. **39**, 3378-3381 (2014).

15. C.-H. Wang, J. Zhang, M.-Z. Li, Q. Wang, and Z.-S. Gu, "Characteristic of multiply backscatter signal of meteorological Lidar," Acta Photonica Sin. **36**, 1881-1883 (2007).

16. K. Sato, H. Okamoto, and H. Ishimoto, "Modeling Lidar multiple scattering," EPJ Web Conf. **119**, 21005 (2016).

17. H. Zhang, L. Bu, H. Gao, X. Huang, and K. R. Kumar, "Retrieving homogeneous liquid cloud microphysical proper using multiple-field-of-view Lidar," J. Appl. Remote Sens. **12**, 046021 (2018).

18. H. Okamoto, K. Sato, T. Nishizawa, N. Sugimoto, and Y. Jin, "Development of multiple scattering polarization Lidar to observe depolarization ratio of optically thick low level clouds," AIP Conf. Proc. **1810**, 050002 (2017).

19. X. Sun, S. Xiao, L. Wan, H. Wang, and J. Sun, "Monte Carlo simulation of polarization Lidar multiple scattering ndepolarization by water cloud," Chin. J. Laser **42**, 232-239 (2015).

20. S. R. D. Roode and A. Los, "The effect of temperature and humidity fluctuations on the liquid water path of non-precipitating closed cell stratocumulus clouds," Q. J. R. Meteorol. Soc. **134**, 403-416 (2008).

21. V. Freudenthaler, M. Esselborn, M. Wiegner, B. Heese, M. Tesche, A. Ansmann, D. MüLLER, D. Althausen, M. Wirth, A. Fix, G. Ehret, P. Knippertz, C. Toledano, J. Gasteiger, M. Garhammer, and M Seefeldner, "Depolarization ratio profiling at several wavelengths in pure Saharan dust during SAMUM 2006," Tellus B **61**, 165-179 (2009).

22. L. Bu, R. Sa, and D. Kim, "Calibration method of polarization Lidar based on Jones matrix," Optik **130**, 834-839 (2017).

23. M. Hayman and J. P. Thayer, "Explicit description of polarization coupling in Lidar applications," Opt. Lett. **34,** 611-613 (2009).

24. K. Sassen, "The polarization Lidar technique for cloud research: a review and current assessment," Bull. Am. Meteorol. Soc. **72**, 1848-1866 (1992).

25. K. Osródka and J. Szturc, "Quality-based generation of weather radar Cartesian products," Atmos. Meas. Tech. **8**, 2173-2181 (2015).